RSC Advances

ROYAL SOCIETY OF CHEMISTRY

www.rsc.org/advances

Journal Name

ARTICLE

Facile preparation of yolk-shell structured Si/SiC@C@TiO_2 nanocomposites as highly efficient photocatalysts for degrading organic dye in wastewater †

Received 00th January 20xx,
Accepted 00th January 20xx

DOI: 10.1039/x0xx00000x

www.rsc.org/

Mei-Pin Liu[a], Tingting Su[a], Lin Sun[a] and Hong-Bin Du[a,*]

The yolk-shell structured Si/SiC@C (YSSC) nanospheres were prepared by a facile magnesiothermic reduction process. After coating with TiO_2 nanoparticles, the YSSC@TiO_2 composites possess a Brunauer–Emmett–Teller (BET) and Langmuir surface area of 423 and 584 $m^2 g^{-1}$, respectively, and show high adsorption capability for methyl blue (MB) and Congo red in water. Moreover, the nanocomposites show a strong photon absorbance throughout the visible light region, and exhibit excellent photocatalytic performance for degrading MB in water. The MB degradation follows the pseudo 1st order kinetics and the calculated rate constant for YSSC@TiO_2 under UV (visible) light irradiation is approximately 4.5 (7.9), 8 (17), and 7.6 (22.7) times larger than that of the synthesized TiO_2, commercial P25 and YSSC spheres, respectively. Stability tests show that the YSSC@TiO_2 nanospheres possess high stability and maintain good photocatalytic activity over four times of cycle experiments. The excellent photocatalytic activity of YSSC@TiO_2 can be ascribed to the synergism of high adsorption of dye molecules on the surface, extended light adsorption range and the formation of semiconductor heterostructures that allow for efficient separation of photogenerated electrons and holes through a Z-scheme system within the catalyst.

1. Introduction

Nowadays, widely dispersed organic wastes such as dyes and pigments in the industries have been considered as environmental hazards and priority pollutants of wastewater by many countries because of their long lasting persistence and high toxicity.[1] These pollutants must be degraded to below environmentally accepted levels before discharging to public rivers. Various technologies have been developed to address this problem, such as adsorption,[2, 3] biodegradation treatment,[4] advanced and catalytic oxidation processes,[5] and so on.[6] Recently, photocatalytic degradation combined with adsorption technique has attracted much attention because of its high efficiency and extensive applicability for most organic compounds. Titania is the most widely investigated photocatalyst due to its high photocatalytic efficiency, high chemical stability, nontoxicity and low-cost.[7] However, the photocatalytic degradation activity of TiO_2 is still low to be used for industrial purposes, which results from the faster recombination of the photoinduced electrons and holes in the particles as well as poor solar energy utilization of wide-gap semiconductor TiO_2 ($E_g \approx 3.2$ eV).[8] Therefore, much effort has been made to improve the efficiency of the photocatalytic process and extend the light adsorption range of TiO_2.[9] The widely-used methods include the formation of semiconductor heterostructures (also called Z-scheme photocatalyst),[10] doping,[11] surface hybridization,[12] *etc*.

SiC is a wide bandgap ($E_g \approx 2.4$ eV) material with lightweight, high chemical stability, nontoxicity and high electron mobility.[13] It shows excellent properties in area of energy, photocatalysis, semiconductor and supercapacitor.[14, 15] Several Z-scheme photocatalysts involving SiC have been prepared.[16] For example, SnO_2/SiC hollow sphere nanochains were synthesized and showed the improved catalytic activity in H_2 evolution;[17] Ag_3PO_4/Ag/SiC exhibited enhanced photocatalytic activity in degradation of methyl organic;[18] β-SiC–TiO_2 nanocomposites showed efficient activity in Rhodamine B degradation under solar light.[19] Nevertheless, the photocatalytic activities of these composite photocatalysts still need to be enhanced.

Yolk shell is a hybrid structure of hollow and core/shell structure, with a movable core inside and void space.[20] Yolk-shell nanomaterials usually show good photocatalytic activities since these materials possess high surface area and dye adsorption capacity, and allow the multiple reflections of light within the interior voids.[21] The preparation of SiC with tailored morphology is not trivial, despite that various SiC nanostructures such as nanoparticles, nanorods, nanotubes, nanospheres and mesoporous materials have been prepared by means of high-temperature carbothermal or magnesiothermic reductions,[22] vapor-solid synthesis,[17, 23] polymer-assisted synthesis,[14, 24] *etc*. Herein, we report a facile

[a] *State Key Laboratory of Coordination Chemistry, Collaborative Innovation Center of Chemistry for Life Sciences, School of Chemistry and Chemical Engineering, Nanjing University, Nanjing, 210023, China. E-mail: hbdu@nju.edu.cn.*

† Electronic Supplementary Information (ESI) available: Synthesis, TGA, UV-Vis PXRD patterns and SEM images. See DOI: 10.1039/x0xx00000x

fabrication of a novel yolk-shell structured Si/SiC@C (YSSC) nanospheres by employing the magnesiothermic reduction method at 650 °C for 8 h. The obtained nanospheres not only possess high surface area and high adsorption capability of dye molecules, but also exhibit high photocatalytic activity in the degradation of methyl blue (MB) when coated with TiO_2 to form a Z-scheme photocatalyst. The YSSC and YSSC@TiO_2 nanospheres have been characterized by powder X-ray diffraction (PXRD), X-ray photoelectron spectroscopy (XPS), scanning electron microscope (SEM), transmission electron microscope (TEM), N_2 adsorption and UV-Vis spectroscopic analyses. The adsorption and photocatalytic experiments of organic compounds have been evaluated by using methyl blue (MB) as a model compound.

2. Experimental

2.1 Preparation of SiO_2@RF precursor

Stöber SiO_2 spheres were firstly synthesized according to the literature.[23] Then, the as-prepared SiO_2 spheres were mixed with 70 mL of H_2O and 30 mL of ethanol. 2.3 g of hexadecyltrimethyl ammonium bromide (CTAB) was added into the above mixture, followed by addition of 0.3 g of resorcinol and 0.1 mL of concentrated NH_3 solution. After stirring for about 30 min, 0.5 mL of formaldehyde (40% aqueous solution) was added dropwise into the mixture. The mixture was kept stirring for 8 h. The product was recovered after centrifugation and washed with distilled water several times.

2.2 Preparation of yolk-shell Si/SiC@C nanospheres (YSSC)

0.3 g of the as-prepared SiO_2@RF nanospheres were well mixed with 0.3 g of Mg powders. The mixture was put into a tube furnace and heated to 650 °C for 8 h under a flowing Ar gas (60 mL min^{-1}). The obtained solids were washed with 2 M HCl and HF (5%) solution several times. The black products (0.13 g) were obtained after dried under vacuum at 70 °C.

2.3 Preparation of YSSC@TiO_2 spheres

0.1 g of 1-hexadecylamine and 0.06 mL of 0.1 M KCl solution were dissolved in 15 mL of ethanol. To the above solution were added 0.04 g of the as-prepared YSSC spheres. After stirring for 10 min, titanium tetraisopropanolate (1 mmol, 1.0 mL) was added dropwise into the mixture. The mixture was continually stirred for 1 h and aged at room temperature for 24 h. The gray precipitate was collected by centrifugation, washed with deionized water and ethanol for 3 times and calcined in Ar at 500°C for 2 h. For comparison, TiO_2 was prepared through a similar method without adding YSSC spheres; and carbon spheres in C@TiO_2 was synthesized in absence of Mg during the preparation of YSSC spheres.

2.4 Characterization methods

PXRD patterns were collected in the 2θ = 5-50° range with a scan speed of 0.1 s/deg on a Bruker D8 Advance instrument using a Cu Kα radiation at RT. SEM images were obtained on a Hitachi S-4800 field-emission scanning electron microscope at an acceleration voltage of 5.0 kV. TEM images were obtained on a JEM-200CX transmission electron microscope. Thermogravimetric (TG) analyses were performed on a simultaneous STA449F3 thermal analyser under a flowing oxygen. X-ray photoelectron spectroscopy (XPS) measurements were recorded with a PHI 5000 VersaProbe. A Micromeritics ASAP 2020 surface area porosimetry system was used to measure gas adsorption. Before the measurements, the samples were activated at 200°C for 5 h under dynamic vacuum. UV-Vis diffuse reflectance spectra were recorded on a Perkin-Elmer Lambda 950 UV/VIS/NIR spectrometer. The UV-Vis spectroscopy was carried on a Shimadzu UV-3600 spectrophotometer.

2.5 Adsorption of dyes

Congo red (CR) and methyl blue (MB) were selected as organic pollutant models. Typically, the YSSC spheres (500 mg L^{-1}) were mixed with 40 mL of 200 mg L^{-1} CR or MB solutions. After intervals of stirring, 2 mL of aliquots were collected and centrifuged; the solutions were analyzed by UV–Vis spectroscopy.

2.6 Photocatalytic test

Photocatalytic experiments were studied by degradation of MB solution. Ultraviolet lamp (~365 nm, 30 W) and Xe lamp (TIPX 5002, SOFN Instruments Co. Ltd.) were used as light sources. 50 mL of MB solution (120 mg L^{-1}) and 10 mg of solid catalyst were mixed. Before starting the photocatalytic reaction, the solution was stirred under darkness for 30 min to reach the equilibrium. 2 mL of the solution were collected from the suspension in every 5 minutes and centrifuged. The concentration of MB was measured on a UV-Vis spectrophotometer.

3. Results and Discussion

3.1 Characterization of YSSC

As shown in Fig. 1a, the SiO_2@RF precursors consist of monodispersed nanospheres with a diameter of *ca*. 300 nm. The thickness of the resin layer is about 27 nm. After magnesiothermic reduction and treatments with dilute HCl and HF, the obtained SiC/Si@C (YSSC) spheres retain the spherical morphology (Fig. 1b-c). The spheres are of yolk-shell structure as evidenced from some broken spheres as well as the TEM images. The hollow spheres are covered with a *ca*. 21 nm thickness of carbon layer. TGA studies showed that the YSSC spheres consist of about 8.2 wt% of amorphous carbon (Fig. S1, ESI).

As depicted in Fig. 1f, PXRD studies show that the obtained yolk-shell YSSC samples consist of crystalline Si and β-SiC phases. The three peaks at 2θ = 28.4°, 47.3° and 56.1° can be assigned to the (111), (220) and (311) planes, respectively, of a cubic phase silicon (JCPDS 27-1402) with a = 5.4306 Å. The peaks at 2θ = 35.6°, 41.3° and 60.0° are contributed to the (111), (200) and (220) planes of β-SiC (JCPDS 65-0360, a = 4.3584 Å). Furthermore, two types of lattice fringes are clearly

observed in the high-resolution TEM images (Fig. 1c). The measured d-spacings are 0.252(1) nm and 0.310(1) nm, respectively, which can be attributed to the (111) lattice plane of β-SiC and Si. These results are in good agreement with those of the PXRD studies, which give rise to the (111)-spacings of 0.2516 and 0.3130 nm for β-SiC and Si, respectively.

Fig. 1g shows N_2 adsorption and desorption isotherms of the YSSC spheres. The isotherms are of type IV with a hysteresis ring, suggesting the presence of micropores and mesopores. The Brunauer–Emmett–Teller (BET) and Langmuir surface area of YSSC are 143 and 198 $m^2\ g^{-1}$, respectively. The calculated BJH pore diameter of YSSC spheres based on desorption curves is about 3.6 nm. Owing to the high specific surface area, large pore size, good thermal and chemical stability, the YSSC spheres could be used as efficient adsorbents for large molecules. To confirm it, the adsorption of methyl blue (MB) and Congo red (CR) in the water over the YSSC spheres were tested. As shown in Fig. 1h, the YSSC spheres demonstrated high adsorption capacities of 269 and 368 mg g^{-1} towards CR and MB, respectively, much higher than other porous core-shell materials reported in the literature, such as core-shell Fe_3O_4@MIL-100(Fe) (MB, 49.4 mg g^{-1}),[26] core-shell C@Al_2O_3 (Orange-II, 108 mg g^{-1}),[2] core-shell γ-MnO_2/α-MnO_2 (MB, 62 mg g^{-1}),[27] and multi-wall carbon nanotube (CR, 140 mg g^{-1}).[28] These results have shown the YSSC spheres could be promising candidates for removing toxic pollutants from waste water.

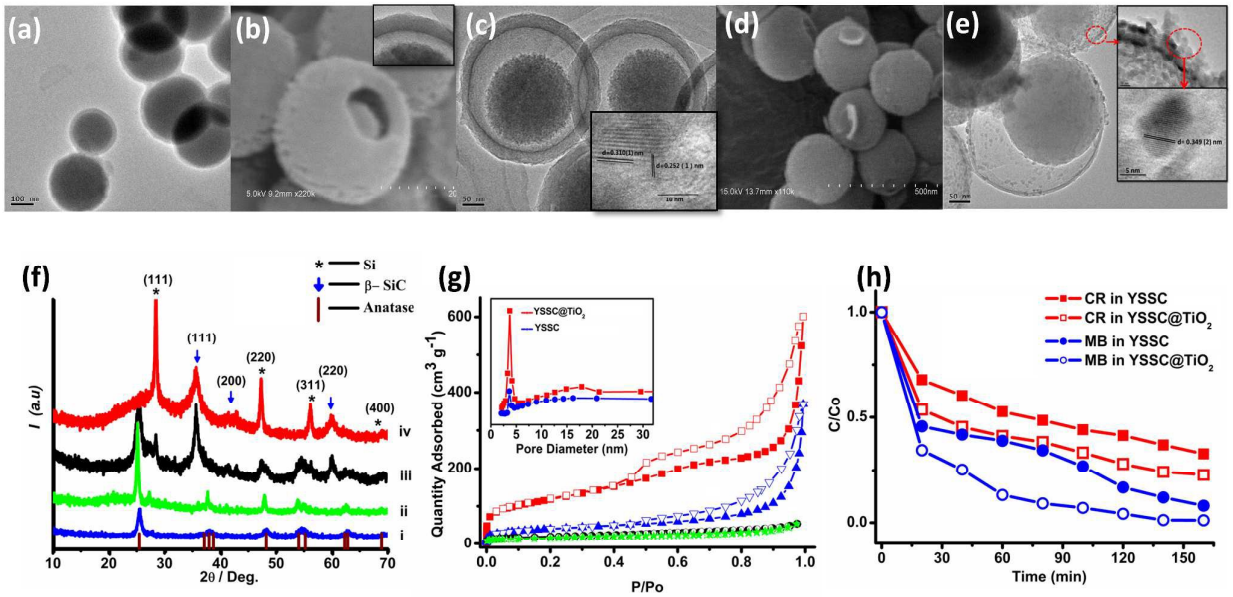

Fig. 1 (a) TEM image of precursor SiO_2@RF nanospheres; (b) SEM and (c) TEM images of YSSC nanospheres (inserts are the HRTEM images); (d) SEM and (e) TEM images of YSSC@TiO_2 nanospheres (inserts are HRTEM images). (f) PXRD of synthesized TiO_2 (i), P25 (ii), YSSC@TiO_2 nanospheres (iii) and YSSC nanospheres (iv); (g) N_2 adsorption (solid symbols) and desorption (empty symbols) isotherms of YSSC@TiO_2 nanospheres (Squares), YSSC nanospheres (Triangles), synthesized TiO_2 (Circles) and P25 (Stars). Insert is the BJH pore distribution curves of YSSC@TiO_2 (red squares) and YSSC nanospheres (blue circles); (h) Adsorption profiles of YSSC (Solid symbols) and YSSC@TiO_2 (Empty symbols) for MB (Circles) and CR (Squares) in water.

3.2 Characterization of YSSC@TiO_2.

Fig. 1f shows the PXRD patterns of the YSSC@TiO_2 sample. Besides those peaks of crystalline silicon and silicon carbide, the rest diffraction peaks could be indexed to anatase TiO_2 (JCPDS 21-1272). The SEM and TEM images of YSSC@TiO_2 in Fig. 1 d-e show that the spheres maintain the yolk-shell morphology with small TiO_2 nanocrystallites of about 10-15 nm in size coated on the surface of the YSSC spheres. Lattice fringes of TiO_2 nanocrystallites could be clearly seen in the HR-TEM images in Fig. 2e. The calculated d-spacings is *ca*. 0.349(2) nm, which corresponds to the (101) lattice plane of anatase TiO_2 shown in PXRD studies ($2\theta = 25.28^o$, d-spacing = 0.351(1) nm).

The N_2 adsorption and desorption isotherms of the YSSC@TiO_2 spheres are similar to those of the YSSC spheres (Fig. 1g), but with larger N_2 adsorption capacity. The isotherms are also of type IV with a hysteresis ring, suggesting the presence of micropores and mesopores. The Brunauer–Emmett–Teller (BET) and Langmuir surface areas of YSSC@TiO_2 are 423, and 584 $m^2\ g^{-1}$, respectively, larger than those of the YSSC spheres. The calculated BJH pore diameter of the YSSC@TiO_2 spheres based on desorption curves is about 3.7 nm, which is similar to that of the uncoated YSSC spheres. As shown in Fig. 1h, the YSSC@TiO_2 spheres demonstrated higher adsorption capacities of dyes in water compared to the YSSC spheres, taking up *ca.* 312 and 395 mg g^{-1} of CR and MB from wastewater, respectively.

The survey of XPS spectra was carried out to confirm the compositions of the YSSC@TiO_2 spheres. From Fig. 2a, one can find the strong signals of C 1s, Ti 2p, O 1s as well as the peak of Si 2p. High resolution XPS peaks of C 1s (Fig. 2b) show the binding energy peaks at 282.8, 284.2 and 283.8 eV, attributable to the signals of Si–C, C=C and C–O–Ti,

respectively.[29-31] The O 1s XPS spectrum in Fig. 2c reveals the signals of Ti–O at 529.0 and 529.4 eV, and the O–C peak at 531.2 eV, respectively.[19, 32] The peaks at 99.3 and 100.8 eV in Si 2p XPS spectrum (Fig. 2d) are highly consistent with the Si–Si and Si–C bonding.[29, 33] In addition, the weak peak at 102.4 eV could be assigned to the Ti–O–Si linkage.[19] Two peaks at 458.0 and 463.6 eV in Ti 2p XPS spectrum are attributed to those of Ti $2p_{3/2}$ and Ti $2p_{1/2}$, respectively (Fig. 2f).[30] These results are consistent with the PXRD results, showing the presence of TiO_2, SiC, Si and C in the spheres. Moreover, the results demonstrate the intimate contacts between them *via* Si–C, C–O–Ti and Ti–O–Si bonds, forming semiconductor heterojunctions. Based on the XPS spectra, the estimated mole ratios of Si, SiC, and TiO_2 in YSSC@TiO_2 are 1 : 1.24 : 4.48.

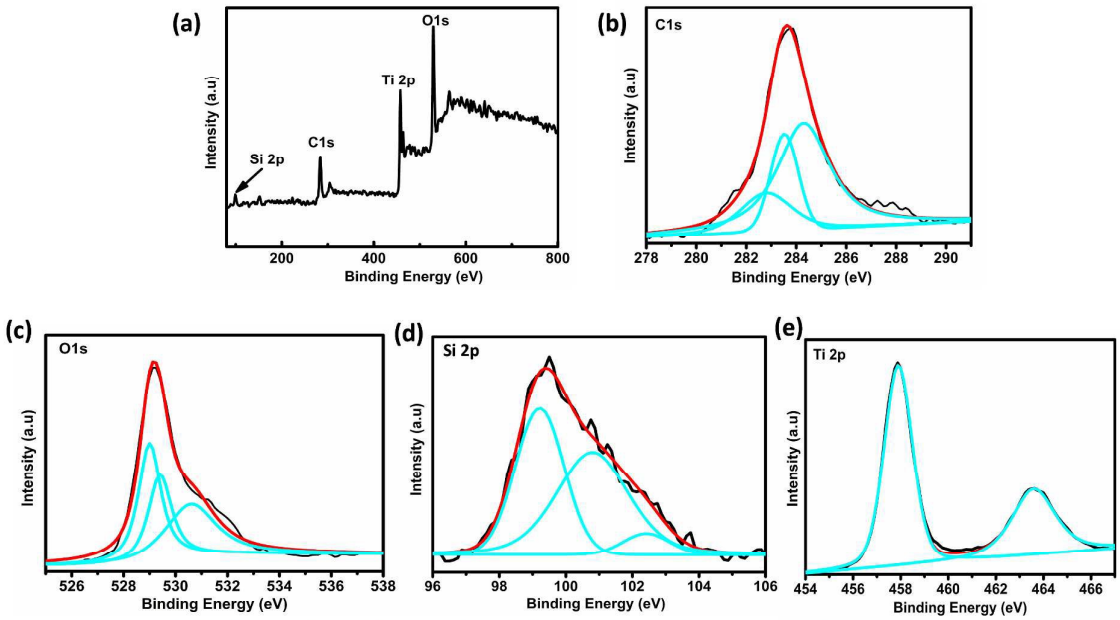

Fig. 2 XPS spectra of YSSC@TiO_2 nanospheres: (a) full range, (b) C 1s, (c) O 1s, (d) Si 2p, and (e) Ti 2p regions

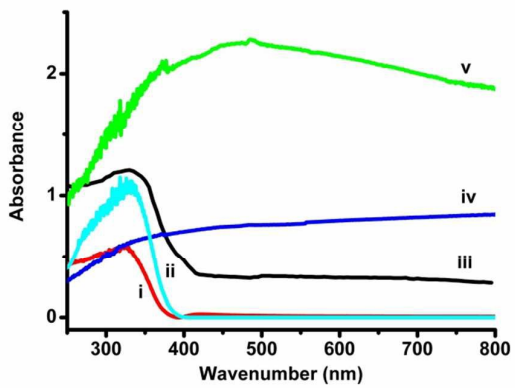

Fig.3 UV-Vis diffuse reflectance spectra of P25 (i), synthesized TiO_2 (ii), C@TiO_2 (iii), YSSC (iv) and YSSC@TiO_2 (v).

The steady-state optical property of YSSC@TiO_2 was investigated by UV-Vis absorbance spectroscopy. The neat, as-prepared TiO_2 and commercial P25 were used as blank for comparisons. As shown in Fig. 3, the as-prepared TiO_2 and commercial P25 exhibit no absorption in visible light region. On the other hand, the YSSC and YSSC@TiO_2 spheres show an enhanced absorbance throughout the visible light region, which could be attributed to the existence of Si and SiC with a narrower bandgap of 1.12 eV and 2.2 eV, respectively. From the UV-Vis absorbance data, the bandgap energy can be deduced from plots of $(\alpha h\nu)^{1/2}$ *versus* energy ($h\nu$), where α is absorption coefficient, and $h\nu$ is photon energy.[32] As shown in Fig. S2 (ESI), the calculated bandgap energies of P25, blank TiO_2 and C@TiO_2 are 3.11, 2.87 eV and 2.79 eV, respectively, while that of YSSC@TiO_2 is 1.39 eV.

3.3 Photocatalytic activities

Methyl blue (MB) was selected as a pollutant model in water to evaluate the photocatalytic activities of the as-synthesized YSSC@TiO_2 under UV and visible lights. For comparisons, the photocatalytic degradation of MB in water over commercial TiO_2 (Degussa P25, ~80 nm in size, Fig. S3), synthesized anatase TiO_2 (~60 nm in size), C@TiO_2 (hollow spheres), YSSC and 5:1 (mass ratio) mixture of anatase TiO_2 and YSSC (denoted YSSC–TiO_2) were also investigated by using the same amount of TiO_2 or YSSC. The results are presented in Fig. 4. Under darkness, physical adsorption of dye molecules over the catalysts occurs. The adsorption capacities follow the order of YSSC@TiO_2 > C@TiO_2> YSSC–TiO_2 ≈ YSSC > synthesized TiO_2 > P25, which are in consistent with the order of their specific BET surface areas, *i.e*. 423, 173, 151, 143, 68, and 49 $m^2\ g^{-1}$, respectively. The YSSC@TiO_2 composites showed the largest adsorption capacity of ~40% for removing MB from water after 30 min of equilibrium, followed by the C@TiO_2 spheres and YSSC–TiO_2 physical mixtures. With the light on, the photocatalytic degradation of MB takes place. As

shown in Fig. 4a, the percentage of MB removal under UV light irradiation follows the order of YSSC@TiO_2 > C@TiO_2 > YSSC–TiO_2 > synthesized TiO_2 > YSSC > P25. However, taking account of physical adsorption, the photocatalytic degradation of MB would follow the order of YSSC@TiO_2 > C@TiO_2 > synthesized TiO_2 > YSSC–TiO_2 > YSSC ≈ P25. In other words, the YSSC@TiO_2 is the most efficient photocatalyst in degrading dyes in water, while the P25 and YSSC spheres are the least efficient. After removal of ~40% MB in water by physical adsorption, about 90% of the rest MB were degraded over YSSC@TiO_2 under UV irradiation within 30 min. Under the identical conditions, however, only approximately 42, 36, 31, 24 and 22% of the rest MB were degraded under UV light irradiation by C@TiO_2, synthesized TiO_2, YSSC–TiO_2, YSSC and P25, respectively. Similar trends have been observed for photocatalytic degradation of MB over these catalysts under visible light irradiation. As shown in Fig. 4c, the photocatalytic degradation of MB follows the same order of YSSC@TiO_2 > C@TiO_2 > synthesized TiO_2 > YSSC–TiO_2 > YSSC ≈ P25, with 82, 35, 20, 16, 10, and 8% of the rest MB dye degraded under visible light irradiation, respectively. It is noted that the catalysts, particularly the TiO_2 and YSSC–TiO_2, exhibited lower photodegrading efficiencies under visible light than UV light, which is mainly due to the poor solar energy utilization of wide-gap semiconductor TiO_2. These results indicate that TiO_2 is the main active ingredient for photocatalytic degradation of MB, and the YSSC@TiO_2 catalyst likely forms semiconductor heterostructures that exhibit the most efficient activity in MB degradation.

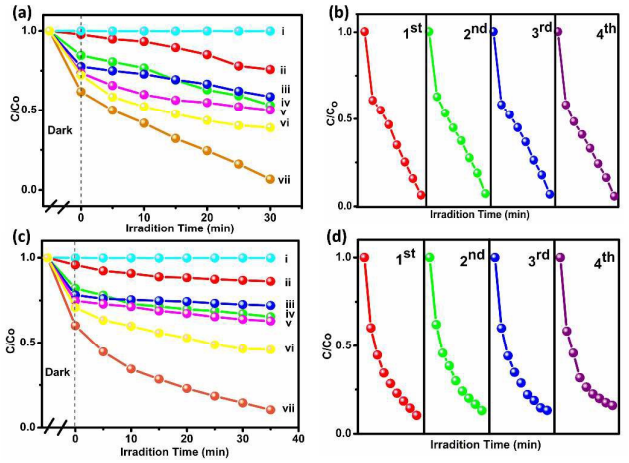

Fig. 4 Comparison of photocatalytic activities towards MB degradation under (a) UV and (b) visible light irradiation: (i) without catalyst, (ii) P25, (iii) YSSC nanospheres, (iv) synthesized TiO_2, (v) YSSC–TiO_2, (vi) C@TiO_2 and (vii) YSSC@TiO_2; Recycling tests of YSSC@TiO_2 for the degradation of MB under (b) UV and (d) visible light irradiation.

The stability and reusability of the photocatalysts are very important factors for their utilization in sustainable environmental technology. Therefore, the cycling degradation experiments over the YSSC@TiO_2 catalyst were evaluated and the results are shown in Fig. 4b and 4d. The YSSC@TiO_2 photocatalyst do not display an obvious decrease in photocatalytic degradation activity after 4 cycles. PXRD studies showed that the crystalline structure of the used catalyst kept intact (Fig. S4). The SEM image (Fig. S5) shows that the morphology of the hollow spheres of the catalyst still retained after the recycling reactions. These results indicate that the YSSC@TiO_2 photocatalyst possesses high stability and can be easily recovered for reuse in photocatalytic degradation of organic pollutants.

The kinetics of MB degradation were investigated by using the Langmuir-Hinshelwood model,[35, 36] *i.e.* $\ln(C_o/C) = kt$, where k is the pseudo-first order rate constant, C and C_o are concentration of dye at time t and t = 0, respectively. The results are summarized in Table 1. This equation fits reasonably well with the experimental data with all the R^2 values greater than 0.9, which suggests that the MB degradation over these catalysts follow the pseudo 1st order kinetics. The calculated rate constant k_1 value for YSSC@TiO_2 under UV light is 0.0703 min^{-1}, approximately 3.5, 4.5, 5.7, 7.6 and 8 times larger than that of the C@TiO_2, synthesized TiO_2, YSSC–TiO_2 mixtures, YSSC spheres and commercial P25, respectively. Similarly, the k_2 value for YSSC@TiO_2 under visible light is 0.0476 min^{-1}, 3.8, 7.9, 9.3, 22.7, and 17 times larger than the C@TiO_2, synthesized TiO_2, YSSC–TiO_2 mixtures, YSSC spheres and commercial P25, respectively. These results confirm that the composite YSSC@TiO_2 nanospheres have the best photocatalytic activity.

Table 1 Pseudo-1st order kinetics of MB degradation over various catalysts under UV light (k_1) and visible light irradiation (k_2).

Catalyst	k_1 (min^{-1})	R_1^2	k_2 (min^{-1})	R_2^2
YSSC@TiO_2	0.0703	0.91	0.0476	0.99
C@TiO_2	0.0199	0.95	0.0125	0.97
Synthesized TiO_2	0.0157	0.99	0.0060	0.94
YSSC–TiO_2	0.0123	0.98	0.0051	0.99
YSSC	0.0093	0.98	0.0021	0.96
P25	0.0089	0.96	0.0028	0.91

The excellent photocatalytic activity of YSSC@TiO_2 can be attributed to its unique structure and composition. Firstly, the catalyst consists of yolk-shell structured nanospheres coated with TiO_2 nanoparticles. It possesses large BET surface area of 423 m^2 g^{-1} with mesopores of *ca*. 3.7 nm in diameter, and can adsorb up to 395 mg g^{-1} of MB in water. The high adsorption ability of the YSSC@TiO_2 spheres is definitely a positive aspect in degradation process,[37] because the photocatalytic reactions only occur on the active sites of the semiconductor surface and the dyes adsorbed on the surface can thus be degraded *in situ* rapidly without the prior diffusion. The yolk-shell structure of YSSC@TiO_2, on the other hand, may allow the multiple reflections of light within the interior voids during the photocatalytic reactions,[21] thus leading to improved activities. Secondly, the catalyst is made up of narrower band gap semiconductors Si and SiC besides the wide band gap TiO_2 nanoparticles. It shows a strong photon absorbance

throughout the visible light region. The extended light absorbance will improve the solar energy utilization and thus enhance the efficiency of the photocatalyst. Thirdly, the semiconductors Si, SiC and TiO_2 are intimately contacted with each other *via* Si–C, C–O–Ti and Ti–O–Si bonds (Fig. 2 and Fig. S6), forming semiconductor heterojunctions as observed in many other heterojunction nanocomposites.[17,19,36,38] When the semiconductors are excited by lights to generate holes and electrons in their conduction and valence bands, respectively, the electrons on the conduction band minimum of Si and SiC can easily diffuse into TiO_2 through the Schottky barrier, with holes remained in the valence band of SiC and Si. Through the junction of the TiO_2 and SiC/Si interface, the electron-hole pairs could be easily separated and thus result in a reduced e^-–h^+ recombination. The electrons accumulated on the surface of TiO_2 are scavenged by adsorbed O_2 to generate super oxide radicals, which are responsible for the degradation of the MB. As results, YSSC@TiO_2 is a Z-scheme photocatalyst that exhibits high catalytic activity in the degradation of MB in wastewater.

4. Conclusions

In summary, yolk-shell structured Si/SiC@C (YSSC) nanospheres were successfully prepared through a simple magnesiothermic reduction route. When coated with TiO_2 on the surface, the formed YSSC@TiO_2 nanocomposite possesses large specific surface area and exhibits high adsorption capacity for dye molecules from wastewater. Furthermore, it exhibits a strong photon absorbance throughout the visible light region, and is highly photocatalytic active for degradation of organic dye MB in wastewater. This robust, reusable, and environmental benign material of YSSC@TiO_2 may be of use in addressing environmental issues for sustainable development, such as wastewater treatment.

Acknowledgements

We are grateful for financial support from the National Natural Science Foundation of China (21471075) and Program B for Outstanding PhD Candidate of Nanjing University.

Notes and references

1 Y. Patino, E. Diaz, S. Ordonez, E. Gallegos-Suarez, A. Guerrero-Ruiz and I. Rodriguez-Ramos, *Chemosphere*, 2015, **136**, 174; B. Thokchom, A. B. Pandit, P. Qiu, B. Park, J. Choi and J. Khim, *Ultrason. Sonochem.*, 2015, **27**, 210; D. Shahidi, R. Roy and A. Azzouz, *Appl. Catal. B*, 2015, **174**, 277.

2 J. Zhou, C. Tang, B. Cheng, J. Yu and M. Jaroniec, *ACS Appl. Mater. Interfaces*, 2012, **4**, 2174.

3 Z. Wei, R. Xing, X. Zhang, S. Liu, H. Yu and P. Li, *ACS Appl. Mater. Interfaces*, 2013, **5**, 598.

4 P. B. Hatzinger, *Environ. Sci. Technol.,* 2005, **39**, 239a; L. Ye, H. You, J. Yao and H. L. Su, *Desalination*, 2012, **298**, 1.

5 Z. Li, S. Cong and Y. M. Xu, *Acs Catal.*, 2014, **4**, 3273; Q. Sun and Y. M. Xu, *J. Phys. Chem. C*, 2009, **113**, 12387.

6 A. W. Carpenter, C. F. de Lannoy and M. R. Wiesner, *Environ. Sci. Technol.*, 2015, **49**, 5277; T. Bora and J. Dutta, *J. Nanosci. Nanotechnol.*, 2014, **14**, 613.

7 A. A. Ismail and D. W. Bahnemann, *J. Mater. Chem.*, 2011, **21**, 11686; A. Kudo and Y. Miseki, *Chem. Soc. Rev.*, 2009, **38**, 253; X. Lang, X. Chen and J. Zhao, *Chem. Soc. Rev.*, 2014, **43**, 473; J. Ran, J. Zhang, J. Yu, M. Jaroniec and S. Z. Qiao, *Chem. Soc. Rev.*, 2014, **43**, 7787

8 M. Gao, L. Zhu, W. L. Ong, J. Wang and G. W. Ho, *Catal. Sci. Technol.*, 2015, **5**, 4703; M. D. Hernandez-Alonso, F. Fresno, S. Suarez and J. M. Coronado, *Energy Environ. Sci.*, 2009, **2**, 1231.

9 H. Xu, S. Ouyang, L. Liu, P. Reunchan, N. Umezawa and J. Ye, *J. Mater. Chem. A*, 2014, **2**, 12642; Y. Zhang, Z. Jiang, J. Huang, L. Y. Lim, W. Li, J. Deng, D. Gong, Y. Tang, Y. Lai and Z. Chen, *RSC Adv.*, 2015, **5**, 79479.

10 J. Tian, Z. Zhao, A. Kumar, R. I. Boughton and H. Liu, *Chem. Soc. Rev.*, 2014, **43**, 6920.

11 W. J. Zhou, Y. H. Leng, D. M. Hou, H. D. Li, L. G. Li, G. Q. Li, H. Liu and S. W. Chen, *Nanoscale*, 2014, **6**, 4698; J.-Y. Park, K.-H. Lee, B.-S. Kim, C.-S. Kim, S.-E. Lee, K. Okuyama, H.-D. Jang and T.-O. Kim, *RSC Adv.*, 2014, **4**, 9946; X. Wang, K. Zhang, X. Guo, G. Shen and J. Xiang, *New J Chem.*, 2014, **38**, 6139; J. Zhang, Y. Wu, M. Xing, S. A. K. Leghari and S. Sajjad, *Energy Environ. Sci.*, 2010, **3**, 715.

12 K. A. Connelly and H. Idriss, *Green Chem.*, 2012, **14**, 260; Y. Ide, F. Liu, J. Zhang, N. Kawamoto, K. Komaguchi, Y. Bando and D. Golberg, *J. Mater. Chem. A*, 2014, **2**, 4150.

13 D. Q. Zhang, A. Alkhateeb, H. M. Han, H. Mahmood, D. N. McIlroy and M. G. Norton, *Nano Lett.*, 2003, **3**, 983.

14 C. Hoffmann, T. Biemelt, A. Seifert, K. Pinkert, T. Gemming, S. Spange and S. Kaskel, *J. Mater. Chem.*, 2012, **22**, 24841.

15 C. Hoffmann, P. Plate, A. Steinbruck and S. Kaskel, *Catal. Sci. Technol.*, 2015, **5**, 4174; M. Kim and J. Kim, *Phys. Chem. Chem. Phys.*, 2014, **16**, 11323; M. Kim, I. Oh and J. Kim, *Phys. Chem. Chem. Phys.*, 2015, **17**, 4424.

16 Y. Y. Bu, Z. Y. Chen and C. J. Sun, *Appl. Catal. B-Environ.*, 2015, **179**, 363; Y. Y. Chai, J. Ding, L. Wang, Q. Q. Liu, J. Ren and W. L. Dai, *Appl. Catal. B-Environ.*, 2015, **179**, 29; R. Y. Xie, L. P. Zhang, H. Xu, Y. Zhong, X. F. Sui and Z. P. Mao, *J. Mol. Catal. A*, 2015, **406**, 194; Q. Wang, Y. B. Li, T. Hisatomi, M. Nakabayashi, N. Shibata, J. Kubota and K. Domen, *J. Catal.*, 2015, **328**, 308.

17 X. F. Zhou, Y. J. Liu, X. Li, Q. Z. Gao, X. T. Liu and Y. P. Fang, *Chem. Commun.*, 2014, **50**, 1070.

18 Z. H. Chen, F. Bing, Q. Liu, Z. G. Zhang and X. M. Fang, *J. Mater. Chem. A*, 2015, **3**, 4652.

19 G. Mishra, K. M. Parida and S. K. Singh, *RSC Adv.*, 2014, **4**, 12918; G. Sahasrabudhe, S. M. Rupich, J. Jhaveri, A. H. Berg, K. A. Nagamatsu, G. Man, Y. J. Chabal, A. Kahn, S. Wagner, J. C. Sturm and J. Schwartz, *J. Am. Chem. Soc.*, 2015, **137**, 14842.

20 R. Purbia and S. Paria, *Nanoscale*, 2015, **7**, 19789.

21 Q. Xie, J. Li, Q. Tian and R. Shi, *J. Mater. Chem.*, 2012, **22**, 13541; W. Q. Fang, X. H. Yang, H. Zhu, Z. Li, H. Zhao, X. Yao and H. G. Yang, *J. Mater. Chem.*, 2012, **22**, 22082; H. Zhang, M. Ying, R. Gao, L. Hu, Z. Jiao and X. Zhu, *RSC Adv.*, 2015, **5**, 58439; X. Zhang, H. Ren, T. Wang, L. Zhang, L. Li, C. Wang and Z. Su, *J. Mater. Chem.*, 2012, **22**, 13380.

22 X. N. Guo, X. L. Tong, Y. W. Wang, C. M. Chen, G. Q. Jin and X. Y. Guo, *J. Mater. Chem. A*, 2013, **1**, 4657; S. Xie, X. L. Tong, G. Q. Jin, Y. Qin and X. Y. Guo, *J Mater. Chem. A*, 2013, **1**, 2104; P. Yang, X. L. Tong, G. Z. Wang, Z. Gao, X. Y. Guo and Y. Qin, *ACS Appl. Mater. Interfaces*, 2015, **7**, 4772.

23 H. T. Wang, Z. P. Xie, W. Y. Yang, J. Y. Fang and L. N. An, *Cryst. Growth Des.*, 2008, **8**, 3893.

24 J. Yan, A. J. Wang and D. P. Kim, *J. Phys. Chem. B*, 2006, **110**, 5429.

25 W. Stober, A. Fink and E. Bohn, *J. Colloid Interf. Sci.*, 1968, **26**, 62.
26 Y. Shao, L. Zhou, C. Bao, J. Ma, M. Liu and F. Wang, *Chem. Eng. J.*, 2016, **283**, 1127.
27 J. Cao, Q. Mao, L. Shi and Y. Qian, *J. Mater. Chem.*, 2011, **21**, 16210.
28 A. K. Mishra, T. Arockiadoss and S. Ramaprabhu, *Chem. Eng. J.*, 2010, **162**, 1026.
29 S. Contarini, S. P. Howlett, C. Rizzo and B. A. De Angelis, *Appl. Surf. Sci.*, 1991, **51**, 177.
30 R. Bertoncello, A. Casagrande, M. Casarin, A. Glisenti, E. Lanzoni, L. Mirenghi and E. Tondello, *Surf. Interf. Anal.*, 1992, **18**, 525.
31 G. Hopfengärtner, D. Borgmann, I. Rademacher, G. Wedler, E. Hums and G. W. Spitznagel, *J. Electron. Spectrosc.*, 1993, **63**, 91.
32 P. Y. Jouan, M. C. Peignon, C. Cardinaud and G. Lempérière, *Appl. Surf. Sci.*, 1993, **68**, 595; S. Delpeux, F. Beguin, R. Benoit, R. Erre, N. Manolova and I. Rashkov, *Eur. Polym. J.*, 1998, **34**, 905.
33 W. Bensch, O. Helmer, M. Muhler, H. Ebert and M. Knecht, *J. Phys. Chem.*, 1995, **99**, 3326.
34 R. Bajaj, M. Sharma and D. Bahadur, *Dalton T.*, 2013, **42**, 6736.
35 L. Lin, H. Y. Wang, H. M. Luo and P. Xu, *J. Photoch. Photobio. A*, 2015, **307**, 88; C. Sahoo and A. K. Gupta, *J. Environ. Sci. Heal. A*, 2015, **50**, 659.
36 N. Keller, V. Keller, E. Barraud, F. Garin and M. J. Ledoux, *J. Mater. Chem.*, 2004, **14**, 1887.
37 M. Zhang, C. Shao, Z. Guo, Z. Zhang, J. Mu, P. Zhang, T. Cao and Y. Liu, *ACS Appl. Mater. Interfaces*, 2011, **3**, 2573.
38 J. Mukherjee, A. Ranjan, A. K. Saxena, S. Karan, D. K. D. Majumder, A. Ghosh, S. Ghosh, P. K. Das and R. Banerjee, *J. Mater. Chem. C*, 2013, **1**, 6945; G. Mishra, K. M. Parida and S. K. Singh, *ACS Sustain. Chem. Eng.*, 2015, **3**, 245.

Abstract

The yolk-shell structured Si/SiC@C (YSSC) nanospheres were prepared by a facile magnesiothermic reduction process. After coating with TiO_2 nanoparticles, the YSSC@TiO_2 composites possess a Brunauer–Emmett–Teller (BET) and Langmuir surface area of 423 and 584 $m^2\ g^{-1}$, respectively, and show high adsorption capability for methyl blue (MB) and Congo red in water. Moreover, the nanocomposites show a strong photon absorbance throughout the visible light region, and exhibit excellent photocatalytic performance for degrading MB in water under UV light and visible irradiation.